JCTC Journal of Chemical Theory and Computation

pubs.acs.org/JCTC Article

A Nonperturbative Methodology for Simulating Multidimensional Spectra of Multiexcitonic Molecular Systems via Quasiclassical Mapping Hamiltonian Methods

Xing Gao and Eitan Geva*

Cite This: J. Chem. Theory Comput. 2020, 16, 6491−6502

Read Online

ACCESS | Metrics & More | Article Recommendations

ABSTRACT: We present a new methodology for simulating multidimensional electronic spectra of complex multiexcitonic molecular systems within the framework of quasiclassical mapping Hamiltonian (QC/MH) methods. The methodology is meant to be cost-effective for molecular systems with a large number of nuclear degrees of freedom undergoing nonequilibrium nonadiabatic dynamics on multiple coupled anharmonic electronic potential energy surfaces, for which quantum-mechanically exact methods are not feasible. The methodology is based on a nonperturbative approach to field−matter interaction, which mimics the experimental measurement of those nonlinear time-resolved spectra via phase cycling and can accommodate laser pulses of arbitrary shape and intensity. The ability of different QC/MH methods to accurately simulate two-dimensional and pump−probe electronic spectra within the proposed methodology is compared in the context of a biexcitonic benchmark model that includes both the singly excited and doubly excited electronic states. The QC/MH methods compared include five variations of the linearized semiclassical (LSC) method and the mean-field (Ehrenfest) method. The results show that LSC-based methods are significantly more accurate than the mean-field method and can yield quantitatively accurate two-dimensional and pump−probe spectra when nuclear degrees of freedom can be treated as classical-like.

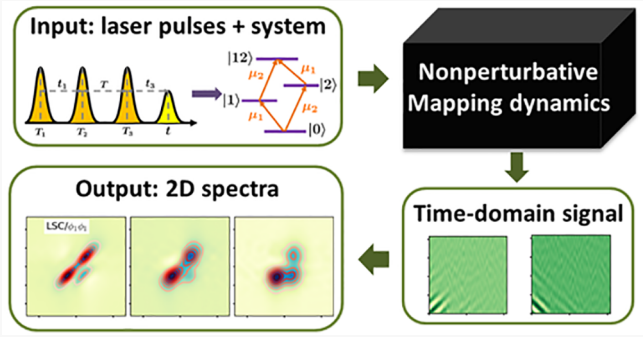

1. INTRODUCTION

Time-resolved nonlinear optical spectroscopy provides a variety of sensitive real time probes of energy and charge transfer dynamics in molecular systems.[1−27] Two-dimensional electronic spectroscopy (2DES), in particular, has emerged over the last two decades as one of the most powerful spectroscopic probes of molecular structure and dynamics.[2−19] Within this technique, one subjects the molecular system to a sequence of three short pulses with controllable interpulse time intervals and individual pulse phases or wave vectors. The heterodyne spectroscopic signal, which corresponds to the expectation value of the dipole moment operator at the detection time, is then measured as a function of the corresponding three time intervals (between the first and second pulses, the second and third pulses, and the third pulse and detection). The overall signal field consists of multiple components that differ with respect to their overall phase or wave vector. 2DES spectra are based on the so-called rephasing and nonrephasing signals that correspond to two specific components of the overall signal field with predetermined overall phases or wave vectors.[1−5]

Resolving the signal field into components based on their overall phase can be achieved by using the method of Seidner et al.,[28] which is analogous to the experimental measurement of those spectra via the phase-cycling method.[29−33] This method is based on simulating the overall signal field for different combinations of interpulse intervals and pulse phases *without treating the field−matter interaction perturbatively*. Components with the overall phase of interest such as the rephasing and nonrephasing signals can then be obtained by performing an inverse Fourier transform (FT).[6,28,33−37]

Arguably, the ultimate goal of modeling 2DES spectra is to translate experimentally measured spectra into an as detailed as possible depiction of the underlying molecular structure and dynamics. In practice, 2DES spectra are often simulated based on models with electronic potential energy surfaces (PESs) that are harmonic and identical, except for shifts in equilibrium geometry and energy.[1,38−45] Within such models, the entire

Received: August 11, 2020
Published: August 31, 2020

https://dx.doi.org/10.1021/acs.jctc.0c00843
J. Chem. Theory Comput. 2020, 16, 6491−6502

information regarding the underlying molecular structure and dynamics is given in terms of spectral density functions.[1,46] Even though harmonic models can often be parametrized so as to reproduce experimental spectra rather well and provide useful insight into their molecular origins, they are still based on a rather restrictive set of assumptions that at the very least need to be validated.[7,45,47−49] Furthermore, the spectral density functions represent a rather indirect and nonintuitive connection to the underlying molecular structure and dynamics. Thus, an approach for modeling spectra which is not limited to harmonic model Hamiltonians and is straightforward to apply to complex molecular systems would be highly desirable.[11,13,16−19,50−54] In this paper, we present such an approach, which is based on quasiclassical mapping Hamiltonian (QC/MH) methods.

QC/MH methods have received much recent attention.[55−78] These methods are based on representing the electronic population and coherence operators, whose expectation values correspond to the diagonal and off-diagonal electronic density matrix elements, respectively, in terms of *mapping operators*. Importantly, unlike the original electronic operators, the mapping operators can be given in terms of auxiliary position and momentum operators and as such have a well-defined classical-like limit. Within the QC approximation, one typically treats the nuclear coordinates and momenta, as well as the above-mentioned auxiliary coordinates and momenta associated with the electronic degrees of freedom (DOF), as classical-like. It should be noted that such QC/MH methods are most useful for the study of large systems, especially in the condensed phase, that involve a large number of electronic and/or nuclear DOF and for which quantum-mechanically exact methods are not feasible due to their exponential scaling with system size.[79] Various QC/MH methods have been proposed, which differ with respect to the choice of mapping variables, as well as the sampling used to determine the values of the corresponding electronic variables at different times throughout the dynamics. In this paper, we present a nonperturbative methodology for using QC/MH methods for calculating 2DES spectra and perform a comprehensive comparison of the ability of different QC/MH methods to accurately simulate 2DES spectra of multiexcitonic molecular systems.

It should be noted that several related recent papers have already considered various aspects of the approach under consideration here. One recent study by Provazza and Coker provided an analysis of the ability of the symmetrical quasi-classical (SQC) QC/MH method[62−67,80] to simulate the linear absorption spectra of a biexciton model by using a perturbative strategy with respect to the field matter interaction.[54] Other recent studies by Polley and Loring were based on combining SQC with their optimized mean trajectory approximation to simulate two-dimensional vibronic spectra.[52,53] Yet another recent paper by Gao et al. provided a comprehensive analysis of the ability of different QC/MH methods to calculate linear spectra within perturbative and nonperturbative frameworks.[81] In this paper we extend the analysis in ref 81 to the calculation of 2DES spectra within a nonperturbative framework.

The remainder of this paper is organized as follows. The theory underlying the dynamics of multiexcitonic systems, QC/MH methods, and the simulation of 2DES spectra is outlined in Section 2. The biexciton benchmark model is described in Section 3. Results are presented and discussed in Section 4. A summary of the main results is provided in Section 5.

2. THEORY

2.1. Preliminary Considerations. We consider a system with a total time-dependent Hamiltonian, $\hat{H}(t)$, given by a sum of a time-independent field-free molecular term, $\hat{H}_M$, and a time-dependent field−matter interaction term, $\hat{W}(t)$:

$$\hat{H} = \hat{H}_M + \hat{W}(t) \tag{1}$$

The molecular system is assumed to consist of M coupled two-state chromophores with similar excitation energies (in the sense that the difference between the excitation energies of different chromophores is much smaller than the excitation energies themselves), with the ground and excited states of the jth chromophore given by $|g\rangle_j$ and $|e\rangle_j$, respectively. The corresponding field-free Frenkel exciton Hamiltonian is given by (in what follows, boldfaced variables, for example $\mathbf{A}$, indicate vector quantities, and a hat over a variable, for example $\hat{B}$, indicates an operator quantity):[66,82]

$$\begin{aligned}\hat{H}_M = {} & H_0(\hat{\mathbf{R}}, \hat{\mathbf{P}})|0\rangle\langle 0| + \sum_{j=1}^{M} H_{jj}(\hat{\mathbf{R}}, \hat{\mathbf{P}})|j\rangle\langle j| \\ & + \sum_{j'\neq j}^{M} V_{j'j}(\hat{\mathbf{R}})|j'\rangle\langle j| + \sum_{j'<j}^{M} H_{j'j,j'j}(\hat{\mathbf{R}}, \hat{\mathbf{P}})|jj'\rangle\langle jj'| \\ & + \sum_{j'<j,k'<k}^{M} J_{j'j,k'k}(\hat{\mathbf{R}})|jj'\rangle\langle kk'|\end{aligned} \tag{2}$$

Here $\hat{\mathbf{P}} = \{\hat{\mathbf{P}}_1, \hat{\mathbf{P}}_2, ..., \hat{\mathbf{P}}_{N_n}\}$ and $\hat{\mathbf{R}} = \{\hat{\mathbf{R}}_1, \hat{\mathbf{R}}_2, ..., \hat{\mathbf{R}}_{N_n}\}$ are the mass-weighted coordinates and momenta of the N_n nuclear DOF; $|0\rangle = \prod_{j=1}^{M}|g\rangle_j$ is the ground electronic state (all chromophores are in their ground state); $\{|j\rangle = |e\rangle_j\prod_{j'\neq j}^{M}|g\rangle_{j'}\}$ are the uncoupled singly excited electronic states (the jth chromophore is in its excited state, while all other chromophores are in their ground state); $\{|jj'\rangle = |e\rangle_j\,|e\rangle_{j'}\prod_{m\neq j,j'}^{M}|g\rangle_m\}$ are the uncoupled doubly excited electronic states (the jth and j'th chromophores are in their excited state, while all other chromophores are in their ground state); $\hat{H}_0(\hat{\mathbf{R}}, \hat{\mathbf{P}}) = \hat{\mathbf{P}}^2/2 + V_0(\hat{\mathbf{R}})$ is the ground state nuclear Hamiltonian; $\{\hat{H}_{jj}(\hat{\mathbf{R}}, \hat{\mathbf{P}}) = \hat{\mathbf{P}}^2/2 + V_{jj}(\hat{\mathbf{R}})\}$ are the singly excited states' nuclear Hamiltonians; $\{\hat{H}_{j'j,j'j}(\hat{\mathbf{R}}, \hat{\mathbf{P}}) = \hat{\mathbf{P}}^2/2 + J_{j'j,j'j}(\hat{\mathbf{R}})\}$ are the doubly excited states' nuclear Hamiltonians; $\{V_{j'j}(\hat{\mathbf{R}})\}$ are the nonradiative coupling terms between the singly excited states ($\hat{\mathbf{R}}$-independent when the Condon approximation is applicable); $\{J_{jj'kk'} = \delta_{jk}(1-\delta_{j'k'})V_{j'k'}(\hat{\mathbf{R}}) + \delta_{j'k'}(1-\delta_{jk})V_{jk}(\hat{\mathbf{R}}) + \delta_{jk'}(1-\delta_{j'k})V_{j'k}(\hat{\mathbf{R}}) + \delta_{j'k}(1-\delta_{jk'})V_{jk'}(\hat{\mathbf{R}})\}$ are the nonradiative coupling terms between the doubly excited states ($\hat{\mathbf{R}}$-independent when the Condon approximation is applicable). It should be noted that there are M singly excited states and $M(M-1)/2$ doubly excited states. Also, $|jj'\rangle$ and $|j'j\rangle$ correspond to the same electronic state. The manifold of doubly excited states is included because it is accessible within third-order optical response theory.[1,14] The electronic excitation energies are assumed sufficiently large so that nonradiative coupling terms between different manifolds are negligible.

The field−matter interaction term is given by[1]

$$\hat{W}(t) = -\hat{\boldsymbol{\mu}}\cdot\mathbf{E}(t) \tag{3}$$

Here, $\mathbf{E}(t)$ is the classical driving electric field and $\hat{\boldsymbol{\mu}}$ is the molecular dipole moment operator, which is given by

https://dx.doi.org/10.1021/acs.jctc.0c00843
J. Chem. Theory Comput. 2020, 16, 6491−6502

$$\hat{\boldsymbol{\mu}} = \sum_{j=1}^{M} [\boldsymbol{\mu}_{0j}|0\rangle\langle j| + \boldsymbol{\mu}_{j0}|j\rangle\langle 0|] + \sum_{j\neq j'}^{M} [\boldsymbol{\mu}_{0j}|j'\rangle\langle j'j| + \boldsymbol{\mu}_{j0}|j'j\rangle\langle j'|] \quad (4)$$

where $\boldsymbol{\mu}_{0j} = \langle 0|\hat{\boldsymbol{\mu}}|j\rangle = \langle j'|\hat{\boldsymbol{\mu}}|jj'\rangle$ is the transition dipole moments associated with photoexcitation of the jth chromophore from its ground state to its excited state (assumed $\hat{\mathbf{R}}$-independent within the Condon approximation). It should be noted that only transitions between the ground and the singly excited manifold and between the singly excited manifold and the doubly excited manifold are included in eq 4, which is based on the assumption that the carrier frequency of the radiation field is close to resonance with the individual chromophores excitation energies.

Specializing to the case of 2DES, we assume that $\mathbf{E}(t)$ consists of three short pulses

$$\mathbf{E}(t) = \sum_{n=1}^{3} \boldsymbol{E}_n(t - T_n)\cos[i\omega(t - T_n) - i\mathbf{k}_n\mathbf{r}] \equiv \sum_{n=1}^{3} \boldsymbol{E}_n(t - T_n)\cos[i\omega(t - T_n) - i\phi_n] \quad (5)$$

It should be noted that all three pulses are assumed to have the same carrier frequency, ω, which is assumed to be close to resonance with respect to the transition frequencies of the individual chromophores. The envelope of the nth pulse is given by $\boldsymbol{E}_n(t - T_n) = \boldsymbol{\epsilon}_n g_n(t - T_n)$, where $\boldsymbol{\epsilon}_n$ is the polarization unit vector and $g_n(t - T_n)$ is the temporal profile, which is assumed narrow and centered at time $t = T_n$. $\mathbf{k}_n$ is the wave vector of the nth pulse, which can also be expressed in terms of the phase $\phi_n = \mathbf{k}_n\mathbf{r}$. It is also convenient to define the time intervals between pulses as $t_1 = T_2 - T_1$, $T = T_3 - T_2$, and $t_3 = t - T_3$ which are denoted as coherence, waiting, and detection times respectively (see the left panel of Figure 1).

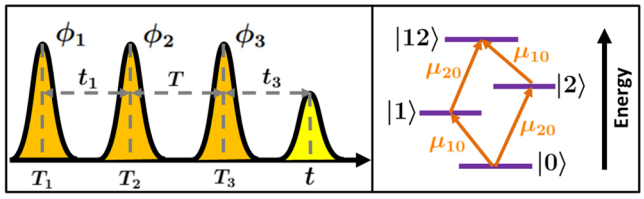

Figure 1. Left panel: Laser pulse sequence used in 2DES (see eq 5). Right panel: Energy level diagram of the biexciton benchmark model system studied in this work. The four energy levels correspond to the ground state ($|0\rangle$), two singly excited states ($|1\rangle$ and $|2\rangle$), and the single doubly excited state ($|12\rangle$). μ_{10} and μ_{20} denote the transition dipole moments.

Substituting eqs 4 and 5 into eq 3 and performing a rotating wave approximation (RWA),[1] we can write the field−matter interaction term in the following form:

$$\hat{W}(t) = -\frac{\hbar}{2}\sum_{j=1}^{M}\sum_{n=1}^{3}[\chi_{0j,n}(t)e^{i\omega t - i(\omega T_n + \phi_n)}|0\rangle\langle j| + \chi_{j0,n}(t)e^{-i\omega t + i(\omega T_n + \phi_n)}|j\rangle\langle 0|] - \frac{\hbar}{2}\sum_{j\neq j'}^{M}\sum_{n=1}^{3}[\chi_{0j,n}(t)e^{i\omega t - i(\omega T_n + \phi_n)}|j'\rangle\langle j'j| + \chi_{j0,n}(t)e^{-i\omega t + i(\omega T_n + \phi_n)}|jj'\rangle\langle j'|] \quad (6)$$

Here $\{\hbar\chi_{0j,n}(t) = \hbar\chi^{*}_{j0,n}(t) = \boldsymbol{\mu}_{0j,n}\cdot\mathbf{E}_n(t)\}$ are the Rabi frequencies associated with the transitions between the ground state and excited state of the jth chromophore, induced by the nth pulse.

2.2. Mixed Quantum-Classical Dynamics in the Rotating Frame. The QC/MH methods under consideration in this paper correspond to a subset of mixed quantum-classical methods, which are based on treating the *nuclear* DOF as classical-like. To this end, we assume that the dynamics of the *electronic* DOF is governed by a *quantum-mechanical* Hamiltonian of the following form:

$$\hat{H}_{el}(\mathbf{R}_t, t) = V_0(\mathbf{R}_t)|0\rangle\langle 0| + \sum_{j=1}^{M} V_{jj}(\mathbf{R}_t)|j\rangle\langle j| + \sum_{j'\neq j}^{M} V_{j'j}(\mathbf{R}_t)|j'\rangle\langle j| + \sum_{j'<j}^{M} J_{j'j,j'j'}(\mathbf{R}_t)|jj'\rangle\langle jj'| + \sum_{j'<j,k'<k}^{M} J_{j'j,k'k}(\mathbf{R}_t)|jj'\rangle\langle kk'| - \frac{\hbar}{2}\sum_{j=1}^{M}\sum_{n=1}^{3}[\chi_{0j,n}(t)e^{i\omega t - i(\omega T_n + \phi_n)}|0\rangle\langle j| + \chi_{j0,n}(t)e^{-i\omega t + i(\omega T_n + \phi_n)}|j\rangle\langle 0|] - \frac{\hbar}{2}\sum_{j<j'}^{M}\sum_{n=1}^{3}[\chi_{0j,n}(t)e^{i\omega t - i(\omega T_n + \phi_n)}|j'\rangle\langle j'j| + \chi_{j0,n}(t)e^{-i\omega t + i(\omega T_n + \phi_n)}|jj'\rangle\langle j'|] \quad (7)$$

Here, $\mathbf{R}_t$ are the nuclear coordinates, which are now described as classical-like and explicitly time-dependent. The actual classical nuclear trajectory, $\mathbf{R}_t$, depends on the choice of mixed quantum-classical method. Furthermore, obtaining a physically meaningful result typically requires averaging over an ensemble of such classical trajectories.[77,83]

In the next step, we define the electronic density operator in the rotating frame, $\tilde{\sigma}(t)$:

$$\tilde{\sigma}(t) = e^{i\hat{H}_{rot}t/\hbar}\hat{\sigma}(t)e^{-i\hat{H}_{rot}t/\hbar} \quad (8)$$

where

$$\hat{H}_{rot} = \hbar\omega\left[\sum_{j=1}^{M}|j\rangle\langle j| + 2\sum_{j'<j}^{M}|jj'\rangle\langle jj'|\right] \quad (9)$$

The equation of motion for $\tilde{\sigma}(t)$ is given by

$$\frac{d}{dt}\tilde{\sigma}(t) = -\frac{i}{\hbar}[\tilde{H}_{el}(\mathbf{R}_t, t), \tilde{\sigma}(t)] \quad (10)$$

https://dx.doi.org/10.1021/acs.jctc.0c00843
J. Chem. Theory Comput. 2020, 16, 6491−6502

where

$$\tilde{H}_{\mathrm{el}}(\mathbf{R}_t, t) = V_0(\mathbf{R}_t)|0\rangle\langle 0| + \sum_{j=1}^{M} \hbar\Delta_{jj}(\mathbf{R}_t)|j\rangle\langle j| + \sum_{j'\neq j}^{M} V_{j'j}(\mathbf{R}_t)|j'\rangle\langle j| + \sum_{j'<j}^{M} \hbar\Delta_{j'j,j'j}(\mathbf{R}_t)|jj'\rangle\langle jj'| + \sum_{j'<j,k'<k}^{M} J_{j'j,k'k}(\mathbf{R}_t)|jj'\rangle\langle kk'| - \frac{\hbar}{2}\sum_{j=1}^{M}\sum_{n=1}^{3}[\chi_{0j,n}(t)e^{-i(\omega T_n+\phi_n)}|0\rangle\langle j| + \chi_{j0,n}(t)e^{i(\omega T_n+\phi_n)}|j\rangle\langle 0|] - \frac{\hbar}{2}\sum_{j\neq j'}^{M}\sum_{n=1}^{3}[\chi_{0j,n}(t)e^{-i(\omega T_n+\phi_n)}|j'\rangle\langle j'j| + \chi_{j0,n}(t)e^{i(\omega T_n+\phi_n)}|jj'\rangle\langle j'|] \quad (11)$$

Here, $\{\Delta_{jj}(\mathbf{R}_t) = V_{jj}(\mathbf{R}_t)/\hbar - \omega\}$ and $\{\Delta_{j'j,j'j}(\mathbf{R}_t) = J_{j'j,j'j}(\mathbf{R}_t)/\hbar - 2\omega\}$ are the instantaneous detunings (the deviations of the transition frequencies from resonance with the carrier frequency of the laser pulse). The main reason for working in the rotating frame is the elimination of the rapidly oscillating factors in the field−matter interaction term, $e^{\pm i\omega t}$ (compare eqs 7 and 11).

2.3. Quasiclassical Mapping Hamiltonian (QC/MH) Methods. For the purpose of this paper, we can restrict ourselves to an initial state of the overall system (electronic + nuclear DOF) of the following single-product form:

$$\hat{\rho}(0) = \hat{\rho}_0^{\mathrm{eq}} \otimes |0\rangle\langle 0| \quad (12)$$

Here, $|0\rangle\langle 0|$ and $\hat{\rho}_0^{\mathrm{eq}} = Z_0^{-1}e^{-\beta\hat{H}_0}$, with $Z_0 = \mathrm{Tr}_n[e^{-\beta\hat{H}_0}]$, are the initial electronic and nuclear density operators, respectively. It should be noted that the nuclear DOF are assumed to start out in ground state thermal equilibrium ($\beta = 1/k_BT$).

Given this initial state, the electronic reduced density matrix elements at a later time t are given by

$$\sigma_{j'j}(t) = \mathrm{Tr}\{\hat{\rho}_0^{\mathrm{eq}}|0\rangle\langle 0|\hat{U}^{\dagger}(t)|j\rangle\langle j'|\hat{U}(t)\} \equiv C_{\hat{M}_{00},\hat{M}_{jj'}}(t) \quad (13)$$

where $\hat{U}(t)$ is the time evolution operator, $\hat{M}_{jj'} = |j\rangle\langle j'|$, and

$$C_{\hat{A}\hat{B}}(t) = \mathrm{Tr}\{\hat{\rho}_0^{\mathrm{eq}}\hat{A}\hat{U}^{\dagger}(t)\hat{B}\hat{U}(t)\} \quad (14)$$

For notation convenience, the double excitation states $\{|jj'\rangle\}$ are also written as $\{|k\rangle\}$ with $k = M+1, ..., (M+1)M/2$, and both notations will be used interchangeably in the following sections. It should be noted that $\hat{A}$ and $\hat{B}$ in eq 14 are purely electronic operators. Thus, calculating $\hat{\sigma}(t)$ calls for calculating the correlation functions $\{C_{\hat{M}_{00},\hat{M}_{jj'}}(t)\}$. It should also be noted that $\{\hat{M}_{jj}\}$ correspond to electronic population operators, and $\{\hat{M}_{jj'}\}$, with $j \neq j'$, correspond to electronic coherence operators. Thus, two kinds of correlation functions contribute to the sum in eq 13: (1) population−population ($j = j'$); (2) population−coherence ($j \neq j'$).

$\{\sigma_{j'j}(t)\}$ can also be written in terms of other sets of correlation functions. One such alternative set, which is particularly useful in the context of MH/QC methods, is based on writing the electronic population operator $\hat{M}_{jj} = |j\rangle\langle j|$ as the sum of the identity operator, $\hat{1}$, and the traceless operator $\hat{Q}_j$:[68,69]

$$\hat{M}_{jj} = \frac{1}{N_e}(\hat{1} + \hat{Q}_j) \quad (15)$$

where $N_e = M + M(M-1)/2 + 1 = M(M+1)/2 + 1$ (the overall number of electronic states) and

$$\hat{Q}_j = N_e\hat{M}_{jj} - \sum_{j'=0}^{N_e-1}\hat{M}_{j'j'} \quad (16)$$

This then gives rise to the following alternative expressions for the population−population and population−coherence correlation functions:

$$C_{\hat{M}_{00},\hat{M}_{jj}}(t) = \frac{1}{N_e^2}[N_e + C_{\hat{1},\hat{Q}_j}(t) + C_{\hat{Q}_0,\hat{Q}_j}(t)] \quad (17)$$

$$C_{\hat{M}_{00},\hat{M}_{jj'}}(t) = \frac{1}{N_e}[C_{\hat{1},\hat{M}_{jj'}}(t) + C_{\hat{Q}_0,\hat{M}_{jj'}}(t)] \quad (18)$$

Thus, $\hat{\sigma}(t)$ can be obtained from two different sets of correlation functions:

$$\text{Set 1: } \{C_{\hat{M}_{00},\hat{M}_{jj}}(t),\ C_{\hat{M}_{00},\hat{M}_{jj'}}(t)\}$$
$$\text{Set 2: } \{C_{\hat{1},\hat{Q}_j}(t),\ C_{\hat{Q}_0,\hat{Q}_j}(t)\} \quad (19)$$

Both sets will yield the exact quantum results if the correlation functions are calculated fully quantum-mechanically. However, this is not the case when approximations methods are used to evaluate the correlation functions (see below).

MH methods are based on representing the population and coherence operators, $\{\hat{M}_{jj'} = |j\rangle\langle j'|\}$, in terms of an isomorphic set of operators, $\{M_{jj'}(\hat{\mathbf{q}}, \hat{\mathbf{p}})\}$:

$$|j\rangle\langle j'| \rightarrow M_{jj'}(\hat{\mathbf{q}}, \hat{\mathbf{p}}) \quad (20)$$

with $\{M_{jj'}(\hat{\mathbf{q}}, \hat{\mathbf{p}})\}$ satisfying the same commutation relations as $\{|j\rangle\langle j'|\}$.[55,57,61,68−74,76,80,84−90] Here, $\{\hat{\mathbf{q}}, \hat{\mathbf{p}}\}$ are a set of auxiliary Cartesian coordinates and momenta operators. Thus, in terms of the mapping operators, the correlation function $C_{\hat{A}\hat{B}}(t)$ (see eq 14) is given by

$$C_{\hat{A}\hat{B}}(t) = \mathrm{Tr}\{\hat{\rho}_0^{\mathrm{eq}}A(\hat{\mathbf{q}}, \hat{\mathbf{p}})B(\hat{\mathbf{q}}_t, \hat{\mathbf{p}}_t)\} \quad (21)$$

where $\hat{\mathbf{q}}_t = \hat{U}^{\dagger}(t)\hat{\mathbf{q}}\hat{U}(t)$ and $\hat{\mathbf{p}}_t = \hat{U}^{\dagger}(t)\hat{\mathbf{p}}\hat{U}(t)$.

Applying the linearized semiclassical (LSC) approximation[91−93] to a correlation function in eq 21 results in the following QC approximation for $C_{\hat{A}\hat{B}}(t)$:

$$C_{A_WB_W}(t) = \left(\frac{1}{2\pi\hbar}\right)^F \int d\mathbf{R}_0 \int d\mathbf{P}_0 \int d\mathbf{q}_0 \int d\mathbf{p}_0 \times [\hat{\rho}_0^{\mathrm{eq}}]_W(\mathbf{R}_0, \mathbf{P}_0)A_W(\mathbf{q}_0, \mathbf{p}_0)B_W(\mathbf{q}_t, \mathbf{p}_t) \quad (22)$$

Here, $F = N_e + N_n$ is the number of DOF of the overall system; $[\hat{\rho}_0^{\mathrm{eq}}]_W(\mathbf{R}_0, \mathbf{P}_0)$ is the Wigner transform of the nuclear operator $\hat{\rho}_0^{\mathrm{eq}}$; $A_W(\mathbf{q}_0, \mathbf{p}_0)$ and $B_W(\mathbf{q}_t, \mathbf{p}_t)$ are the Wigner transforms of the electronic operators $\hat{A}$ and $\hat{B}$, respectively. The general form of the Wigner transforms of a nuclear operator $\hat{D}$ and an electronic operator $\hat{G}$ is given by

https://dx.doi.org/10.1021/acs.jctc.0c00843
J. Chem. Theory Comput. 2020, 16, 6491−6502

$$D_{\mathrm{W}}(\mathbf{R},\mathbf{P}) = \int \mathrm{d}\mathbf{Z} e^{-i\mathbf{Z}\mathbf{P}/\hbar}\left\langle \mathbf{R}+\frac{\mathbf{Z}}{2}\middle| D(\hat{\mathbf{R}},\hat{\mathbf{P}})\middle|\mathbf{R}-\frac{\mathbf{Z}}{2}\right\rangle,$$

$$G_{\mathrm{W}}(\mathbf{q},\mathbf{p}) = \int \mathrm{d}\mathbf{z} e^{-i\mathbf{z}\mathbf{p}/\hbar}\left\langle \mathbf{q}+\frac{\mathbf{z}}{2}\middle| G(\hat{\mathbf{q}},\hat{\mathbf{p}})\middle|\mathbf{q}-\frac{\mathbf{z}}{2}\right\rangle \quad (23)$$

Applying the QC approximation to the two sets of correlation functions in eq 19 then leads to two alternative implementations of the QC/MH approximation (see below).[68,69,77]

The actual choice of mapping variables is not unique, and multiple choices of mapping variables have been proposed and employed.[74,76,80,89,90,94] In this paper, we consider two such choices, which are based on the Stock−Thoss−Meyer−Miller mapping[55,56] (the reader is referred to refs 77 and 95 for a more detailed discussion of these two choices). The first choice, which we refer to as *mapping 1*, leads to the following QC mapping variables:

$$[\hat{M}_{jj}]_{\mathrm{W}}^{(\mathrm{I})}(\mathbf{q},\mathbf{p}) = \frac{1}{2\hbar}(q_j^2+p_j^2-\hbar)$$

$$[\hat{M}_{jj'}]_{\mathrm{W}}^{(\mathrm{I})}(\mathbf{q},\mathbf{p}) = \frac{1}{2\hbar}(q_j-ip_j)(q_{j'}+ip_{j'}) \quad (24)$$

where $j \neq j'$. The second choice, which we refer to as *mapping 2*, leads to the following QC mapping variables:

$$[\hat{M}_{jj}]_{\mathrm{W}}^{(\mathrm{II})}(\mathbf{q},\mathbf{p}) = \phi(\mathbf{q},\mathbf{p})\left(q_j^2+p_j^2-\frac{\hbar}{2}\right)$$

$$[\hat{M}_{jj'}]_{\mathrm{W}}^{(\mathrm{II})}(\mathbf{q},\mathbf{p}) = \phi(\mathbf{q},\mathbf{p})(q_j-ip_j)(q_{j'}+ip_{j'}) \quad (25)$$

where $j \neq j'$ and

$$\phi(\mathbf{q},\mathbf{p}) = \frac{2^{N_e+1}}{\hbar}\exp\left[-\frac{1}{\hbar}\sum_{j=0}^{N_e-1}(q_j^2+p_j^2)\right] \quad (26)$$

We also note that the QC mapping 1 and mapping 2 approximations for $\hat{Q}_j$, eq 16, are given by

$$[\hat{Q}_j]_{\mathrm{W}}^{(\mathrm{I})}(\mathbf{q},\mathbf{p}) = N_e[\hat{M}_{jj}]_{\mathrm{W}}^{(\mathrm{I})}(\mathbf{q},\mathbf{p}) - \sum_{j'=0}^{N_e-1}[\hat{M}_{j'j'}]_{\mathrm{W}}^{(\mathrm{I})}(\mathbf{q},\mathbf{p}),$$

$$[\hat{Q}_j]_{\mathrm{W}}^{(\mathrm{II})}(\mathbf{q},\mathbf{p}) = N_e[\hat{M}_{jj}]_{\mathrm{W}}^{(\mathrm{II})}(\mathbf{q},\mathbf{p}) - \sum_{j'=0}^{N_e-1}[\hat{M}_{j'j'}]_{\mathrm{W}}^{(\mathrm{II})}(\mathbf{q},\mathbf{p}) \quad (27)$$

Applying the above-mentioned QC/MH approximations to the two sets of correlation functions in eq 19 yields the five different LSC-based methods shown in Table 1 (see refs 68, 69, 77 for a more detailed discussion). The first two methods, LSCI (also referred to as PBME[88]) and LSCII (also referred to as LSC-IVR[57]), are based on set 1 of correlation functions (see eq 19). Both LSCI and LSCII use mapping 2 for $[\hat{M}_{00}]_{\mathrm{W}}$ but differ from each other in the mapping used for $[\hat{M}_{jj}]_{\mathrm{W}}$ and $[\hat{M}_{jj'}]_{\mathrm{W}}$, with LSCI using mapping 1 and LSCII using mapping 2. The third through fifth LSC-based methods are based on set 2 of correlation functions (see eq 19).[68] For the correlation functions $C_{[\hat{1}]_{\mathrm{W}}[\hat{Q}_j]_{\mathrm{W}}}$, $C_{[\hat{1}]_{\mathrm{W}}[\hat{M}_{jj'}]_{\mathrm{W}}}$, $C_{[\hat{Q}_0]_{\mathrm{W}}[\hat{Q}_j]_{\mathrm{W}}}$, and $C_{[\hat{Q}_0]_{\mathrm{W}}[\hat{M}_{jj'}]_{\mathrm{W}}}$, all three methods use mapping 2 for $[\hat{Q}_j]_{\mathrm{W}}$ and $[\hat{M}_{jj'}]_{\mathrm{W}}$ but differ in how they map the unity operator and in the mapping used for $[\hat{Q}_0]_{\mathrm{W}}$. The third method, referred to as mLSC/$\phi^1\phi^1$, maps the unity operator onto 1 and uses mapping 1 for $[\hat{Q}_0]_{\mathrm{W}}$. The fourth method, referred to as mLSC/$\phi^1\phi^2$, maps the unity operator onto 1 and uses mapping 2 for $[\hat{Q}_0]_{\mathrm{W}}$. The fifth method, referred to as mLSC/$\phi^2\phi^2$, maps the unity operator onto $2\hbar\phi(\mathbf{q},\mathbf{p})$ [with $\phi(\mathbf{q},\mathbf{p})$ given in eq 26] and uses mapping 2 for $[\hat{Q}_0]_{\mathrm{W}}$.

Table 1. Five LSC-Based QC/MH Methods Used in This Paper[a]

Methods Based on Set 1 in Eq 19		
	$C_{[\hat{M}_{00}]_{\mathrm{W}}[\hat{M}_{jj'}]_{\mathrm{W}}}(t)$	
method	$[\hat{M}_{00}]_{\mathrm{W}}$ mapping	$[\hat{M}_{jj'}]_{\mathrm{W}}$ mapping
LSCI	$[\hat{M}_{00}]_{\mathrm{W}}^{(\mathrm{II})}(\mathbf{q},\mathbf{p})$	$[\hat{M}_{jj'}]_{\mathrm{W}}^{(\mathrm{I})}(\mathbf{q},\mathbf{p})$
LSCII	$[\hat{M}_{00}]_{\mathrm{W}}^{(\mathrm{II})}(\mathbf{q},\mathbf{p})$	$[\hat{M}_{jj'}]_{\mathrm{W}}^{(\mathrm{II})}(\mathbf{q},\mathbf{p})$

Methods Based on Set 2 in Eq 19				
	$C_{[\hat{A}]_{\mathrm{W}}[\hat{B}]_{\mathrm{W}}}(t)$			
	$[\hat{A}]_{\mathrm{W}}$		$[\hat{B}]_{\mathrm{W}}$	
method	$[\hat{1}]_{\mathrm{W}}$ mapping	$[\hat{Q}_0]_{\mathrm{W}}$ mapping	$[\hat{Q}_j]_{\mathrm{W}}$ mapping	$[\hat{M}_{jj'}]_{\mathrm{W}}$ mapping
mLSC/$\phi^1\phi^1$	1	$[\hat{Q}_0]_{\mathrm{W}}^{(\mathrm{I})}(\mathbf{q},\mathbf{p})$	$[\hat{Q}_j]_{\mathrm{W}}^{(\mathrm{II})}(\mathbf{q},\mathbf{p})$	$[\hat{M}_{jj'}]_{\mathrm{W}}^{(\mathrm{II})}(\mathbf{q},\mathbf{p})$
mLSC/$\phi^1\phi^2$	1	$[\hat{Q}_0]_{\mathrm{W}}^{(\mathrm{II})}(\mathbf{q},\mathbf{p})$	$[\hat{Q}_j]_{\mathrm{W}}^{(\mathrm{II})}(\mathbf{q},\mathbf{p})$	$[\hat{M}_{jj'}]_{\mathrm{W}}^{(\mathrm{II})}(\mathbf{q},\mathbf{p})$
mLSC/$\phi^2\phi^2$	$2\hbar\phi(\mathbf{q},\mathbf{p})$	$[\hat{Q}_0]_{\mathrm{W}}^{(\mathrm{II})}(\mathbf{q},\mathbf{p})$	$[\hat{Q}_j]_{\mathrm{W}}^{(\mathrm{II})}(\mathbf{q},\mathbf{p})$	$[\hat{M}_{jj'}]_{\mathrm{W}}^{(\mathrm{II})}(\mathbf{q},\mathbf{p})$

[a] $[\hat{M}]_{\mathrm{W}}^{(\mathrm{I})}$ is given in eq 24, $[\hat{M}]_{\mathrm{W}}^{(\mathrm{II})}$ is given in eq 25, $[\hat{Q}]_{\mathrm{W}}$ is given in eq 27, $\phi(\mathbf{q},\mathbf{p})$ is given in eq 26, and the general form of $C_{A_{\mathrm{W}}B_{\mathrm{W}}}(t)$ is given in eq 22.

In order to obtain the correlation functions in eq 19, the nuclear and electronic coordinates and momenta at time t, $\{\mathbf{R}_t, \mathbf{P}_t, \mathbf{q}_t, \mathbf{p}_t\}$, need to be obtained from the initial state $\{\mathbf{R}_0, \mathbf{P}_0, \mathbf{q}_0, \mathbf{p}_0\}$. The initial nuclear coordinates and momenta, $\{\mathbf{R}_0, \mathbf{P}_0\}$, are sampled from the Wigner transform of the initial nuclear density matrix. The initial electronic coordinates and momenta, $\{\mathbf{q}_0, \mathbf{p}_0\}$, are sampled based on the phase-space density $\phi(\mathbf{q}_0, \mathbf{p}_0)$ or $\phi^2(\mathbf{q}_0, \mathbf{p}_0)$ (see Table 1). $\{\mathbf{R}_t, \mathbf{P}_t, \mathbf{q}_t, \mathbf{p}_t\}$ is obtained from $\{\mathbf{R}_0, \mathbf{P}_0, \mathbf{q}_0, \mathbf{p}_0\}$ via *classical* dynamics as dictated by the following symmetrized mapping Hamiltonian (in the rotating frame):[55,61]

$$\begin{aligned}
\bar{H}(\mathbf{R},\mathbf{P},\mathbf{q},\mathbf{p}) &= \frac{\mathbf{P}^2}{2} + \bar{V}(\mathbf{R}) \\
&+ \frac{1}{2\hbar}[V_0-\bar{V}](\mathbf{R})(q_0^2+p_0^2) + \frac{1}{2}\sum_{j=1}^{M}[\Delta_{jj}-\bar{V}](\mathbf{R})(q_j^2+p_j^2) \\
&+ \frac{1}{2\hbar}\sum_{jj'}^{M} V_{jj'}(\mathbf{R})(q_j-ip_j)(q_{j'}+ip_{j'}) \\
&+ \frac{1}{2}\sum_{j'<j}^{M}[\Delta_{j'j,j'j}(\mathbf{R}_t)-\bar{V}](q_{j'j}^2+p_{j'j}^2) \\
&+ \frac{1}{2\hbar}\sum_{j'<j,k'<k}^{M} J_{j'j,k'k}(\mathbf{R})(q_{jj'}-ip_{jj'})(q_{kk'}+ip_{kk'}) \\
&- \frac{1}{4}\sum_{j=1}^{M}\sum_{n=1}^{3}[\chi_{0j,n}(t)e^{-i(\omega T_n+\phi_n)}(q_0-ip_0)(q_j+ip_j) \\
&+ \chi_{j0,n}(t)e^{i(\omega T_n+\phi_n)}(q_j-ip_j)(q_0+ip_0)] \\
&- \frac{1}{4}\sum_{j<j'}^{M}\sum_{n=1}^{3}[\chi_{0j,n}(t)e^{-i(\omega T_n+\phi_n)}(q_{j'}-ip_{j'})(q_{j'j}+ip_{j'j}) \\
&+ \chi_{j0,n}(t)e^{i(\omega T_n+\phi_n)}(q_{jj'}-ip_{jj'})(q_{j'}+ip_{j'})].
\end{aligned} \quad (28)$$

https://dx.doi.org/10.1021/acs.jctc.0c00843
J. Chem. Theory Comput. 2020, 16, 6491−6502

Table 2. Values of (a, b, c) for the 12 FT Components That Contribute to Optical Response up to Third-Order in Field−Matter Interaction

	1	2	3	4	5	6	7	8	9	10	11	12
a	1	0	0	1	1	−1	2	2	−1	0	−1	0
b	0	1	0	−1	1	1	−1	0	2	2	0	−1
c	0	0	1	1	−1	1	0	−1	0	−1	2	2

It should be noted that the symmetrized form of the mapping Hamiltonian, eq 28, is obtained by defining $\bar{V} = \frac{1}{N_e}\left[V_0 + \sum_{j=1}^{M} \hbar\Delta_{jj} + \sum_{j'<j}^{M} \hbar\Delta_{j'j,j'j}\right]$ and using the closure relation, $\sum_{j=0}^{N_e-1} |j\rangle\langle j| = \hat{1}$.

The mean-field (MF) method can also be cast as a QC/MH-type method.[55] More specifically, given that the initial electronic state is $|\psi(0)\rangle = |0\rangle$, *for a given nuclear trajectory* $\mathbf{R}_t$ the electronic state at a later time t is given by

$$|\psi(t; \mathbf{R}_t)\rangle = \sum_{j=0}^{N_e-1} a_j(t; \mathbf{R}_t)|j\rangle \tag{29}$$

It should be noted that even though the initial electronic state is given by $|0\rangle$ for all nuclear trajectories, different nuclear trajectories will give rise to different $|\psi(t; \mathbf{R}_t)\rangle$.

The corresponding electronic density matrix at time t is then obtained by averaging over the ensemble of nuclear trajectories, which is achieved by averaging over the initial conditions of the nuclear coordinates and momenta based on the Wigner distribution of the initial nuclear density operator:

$$\hat{\sigma}(t) = \left(\frac{1}{2\pi\hbar}\right)^{N_n} \int d\mathbf{R}_0 \int d\mathbf{P}_0 [\hat{\rho}_0^{eq}]_W(\mathbf{R}_0, \mathbf{P}_0) \sum_{j,k=0}^{N_e-1} a_j(t; \mathbf{R}_t) a_k^*(t; \mathbf{R}_t)|j\rangle\langle k| \tag{30}$$

Expressing the expansion coefficients in terms of Cartesian coordinates and momenta as follows

$$a_j = \frac{1}{\sqrt{2}}(q_j + ip_j) \tag{31}$$

it can then be shown that the MF (Ehrenfest) method is equivalent to propagating $\{\mathbf{R}_t, \mathbf{P}_t, \mathbf{q}_t, \mathbf{p}_t\}$ as classical variables whose dynamics are governed by the QC Hamiltonian in eq 28.[55] The initial nuclear coordinates and momenta within the MH method are sampled in the same way as the LSC methods. However, unlike the LSC methods, the initial values of the electronic coordinates and momenta, $\{\mathbf{q}_0, \mathbf{p}_0\}$, are determined by $a_0(0) = (q_0 + ip_0)/\sqrt{2} = 1$ and $a_{j\neq 0}(0) = (q_j + ip_j)/\sqrt{2} = 0$.

2.4. Calculation of Two-Dimensional Spectra. The calculation of 2DES spectra via the QC/MH methods is straightforward within the nonperturbative approach. To this end, we follow the prescription used in ref 96. In this section, we outline the procedure (the reader is referred to refs 28, 34−37, and 96 for a more detailed discussion).

Within the nonperturbative approach, one calculates the expectation value of the dipole moment operator at a time $t > T_3$, as a function of (t_1, T, t_3), for different combinations of pulse phases, (ϕ_1, ϕ_2, ϕ_3) (see Figure 1):

$$\mathcal{P}(\phi_1, \phi_2, \phi_3; t_1, T, t_3) = e^{i\omega t}\left[\sum_{j=1}^{M} \boldsymbol{\mu}_{j0}\tilde{\sigma}_{0j}(t) + \sum_{j<j'}^{M} \mu_{j0}\tilde{\sigma}_{j,jj'}(t)\right] \tag{32}$$

Thus, starting at the initial state in eq 12, calculating $\mathcal{P}(\phi_1, \phi_2, \phi_3; t_1, T, t_3)$ corresponds to simulating the coherences $\{\tilde{\sigma}_{j0}(t), \tilde{\sigma}_{jj',j}(t)\}$ at time $t > T_3$ (following a given sequence of three pulses that correspond to specific choices of time intervals between pulses and the phases of the pulses), which can be done via any of the QC/MH methods outlined in Section 2.3.

Importantly, $\mathcal{P}(\phi_1, \phi_2, \phi_3; t_1, T, t_3)$ can be written in terms of a discrete three-dimensional Fourier transform (FT):

$$\mathcal{P}(\phi_1, \phi_2, \phi_3; t_1, T, t_3) = \sum_{a,b,c} P(a, b, c; t_1, T, t_3) e^{i(a\phi_1 + b\phi_2 + c\phi_3)} \tag{33}$$

where $\{P(a, b, c; t_1, T, t_3)\}$, measuring the emitted signal at direction $a\mathbf{k}_1 + b\mathbf{k}_2 + c\mathbf{k}_3$, is the FT of $\mathcal{P}(\phi_1, \phi_2, \phi_3; t_1, T, t_3)$ and $a, b, c = 0, \pm 1, \pm 2, \pm 3, \ldots$ Thus, $\{P(a, b, c; t_1, T, t_3)\}$ can be obtained via the well-known inverse FT formula from integrals of $\{\mathcal{P}(\phi_1, \phi_2, \phi_3; t_1, T, t_3)e^{-i(a\phi_1 + b\phi_2 + c\phi_3)}\}$ over $\{\phi_1, \phi_2, \phi_3\}$.

2DES spectra are given in terms of two of those FT components, namely $(a, b, c) = (1, -1, 1)$ (the so-called rephasing signal, $P_r(t_1, T, t_3) = P(1, -1, 1; t_1, T, t_3)$) and $(a, b, c) = (-1, 1, 1)$ (the so-called nonrephasing signal, $P_{nr}(t_1, T, t_3) = P(-1, 1, 1; t_1, T, t_3)$):

$$I_{2D}(\omega_1, \omega_3, T) = \mathrm{Re}\int_0^\infty dt_1 \int_0^\infty dt_3 [iP_r(t_1, T, t_3)e^{-i\omega_1 t_1 + i\omega_3 t_3} + iP_{nr}(t_1, T, t_3)e^{i\omega_1 t_1 + i\omega_3 t_3}] \tag{34}$$

Thus, calculating 2DES spectra translates into calculating $P_r(t_1, T, t_3) = P(1,-1, 1; t_1, T, t_3)$ and $P_{nr}(t_1, T, t_3) = P(-1, 1, 1; t_1, T, t_3)$.

It should also be noted that the pump−probe (PP) spectrum corresponds to the case where the first two pulses coincide, so that $t_1 = 0$, and is given by

$$I_{pp}(\omega_3, T) = \mathrm{Re}\int_0^\infty dt_3 iP_{pp}(T, t_3)e^{i\omega_3 t_3} \tag{35}$$

where $P_{pp}(T, t_3) = P_r(t_1 = 0, T, t_3) = P_{nr}(t_1 = 0, T, t_3)$.

Since the quantum-mechanically exact 2DES and PP spectra for the benchmark model that we will test in the methodology in the next section were calculated via the *perturbative* approach,[1] it is convenient to specialize the nonperturbative approach to the case where the field is weak and impulsive. In this limit, it can be shown that optical response up to third-order in the field−matter interaction is given in terms of only the following 12 FT components:[36,96] $\phi_1, \phi_2, \phi_3, 2\phi_1 - \phi_2, 2\phi_2 - \phi_3, 2\phi_1 - \phi_3, 2\phi_2 - \phi_1, 2\phi_3 - \phi_1, 2\phi_3 - \phi_2, -\phi_1 + \phi_2 + \phi_3, \phi_1 - \phi_2 + \phi_3, \phi_1 + \phi_2$

https://dx.doi.org/10.1021/acs.jctc.0c00843
J. Chem. Theory Comput. 2020, 16, 6491−6502

Table 3. 12 Combinations of Phases (ϕ_1, ϕ_2, ϕ_3) Used to Obtain the 12 FT Components in Table 2

	1	2	3	4	5	6	7	8	9	10	11	12
ϕ_1	0	0	$\pi/2$	$\pi/2$	π	π	$(3\pi)/2$	0	0	$\pi/2$	$(3\pi)/2$	$(3\pi)/2$
ϕ_2	0	0	0	0	0	0	0	0	0	0	0	0
ϕ_3	0	$\pi/2$	π	$\pi/2$	0	$\pi/2$	$(3\pi)/2$	$(3\pi)/2$	π	$(3\pi)/2$	π	$\pi/2$

$-\phi_3$ (or equivalently the following 12 possible directions: $\mathbf{k}_1$, $\mathbf{k}_2$, $\mathbf{k}_3$, $2\mathbf{k}_1 - \mathbf{k}_2$, $2\mathbf{k}_2 - \mathbf{k}_3$, $2\mathbf{k}_1 - \mathbf{k}_3$, $2\mathbf{k}_2 - \mathbf{k}_1$, $2\mathbf{k}_3 - \mathbf{k}_1$, $2\mathbf{k}_3 - \mathbf{k}_2$, $-\mathbf{k}_1 + \mathbf{k}_2 + \mathbf{k}_3$, $\mathbf{k}_1 - \mathbf{k}_2 + \mathbf{k}_3$, $\mathbf{k}_1 + \mathbf{k}_2 - \mathbf{k}_3$) (see Table 2). Those 12 FT components can then be obtained from the 12 phase combinations shown in Table 3 by inverting the corresponding 12×12 matrix whose elements are given by $C_{a,b,c;\phi_1,\phi_2,\phi_3} = e^{i(a\phi_1+b\phi_2+c\phi_3)}$ for all the combinations of (a, b, c) and (ϕ_1, ϕ_2, ϕ_3) in Tables 2 and 3, respectively (the reader is referred to ref 96 for the corresponding matrix and its inverse).

3. BENCHMARK MODEL

In the next section, we compare 2DES and PP spectra calculated by applying the six above-mentioned QC/MH methods (LSCI, LSCII, mLSC/$\phi^1\phi^1$, mLSC/$\phi^1\phi^2$, mLSC/$\phi^2\phi^2$, and MF) to a Frenkel biexciton model, for which quantum-mechanically exact results are known. In this section, we outline the model and discuss the choice of parameters.

The Frenkel biexciton model corresponds to the case where the molecular system consists of $M = 2$ chromophores, so that there are $N_e = 4$ electronic states, as shown in Figure 1 (the ground state, $|0\rangle$, two singly excited states, $\{|1\rangle, |2\rangle\}$, and a single doubly excited state, $|12\rangle$). The electronic PESs for these four electronic states are assumed to have the following form:

$$V_0(\mathbf{R}) = \frac{1}{2}\sum_{j=1}^{M}\sum_{\mu=1}^{N}\omega_\mu^2 R_{j,\mu}^2$$

$$V_{jj}(\mathbf{R}) = \epsilon_j + \frac{1}{2}\sum_{\mu}^{N}\omega_\mu^2(R_{j,\mu} - D_\mu)^2 + \frac{1}{2}\sum_{j'\neq j}^{M}\sum_{\mu}^{N}\omega_\mu^2 R_{j',\mu}^2$$

$$J_{jj',jj'}(\mathbf{R}) = \epsilon_j + \epsilon_{j'} + \frac{1}{2}\sum_{\mu}^{N}\omega_\mu^2(R_{j,\mu} - D_\mu)^2 + \frac{1}{2}\sum_{\mu}^{N}\omega_\mu^2(R_{j',\mu} - D_\mu)^2 + \frac{1}{2}\sum_{l\neq j,j'}^{M}\sum_{\mu}^{N}\omega_\mu^2 R_{l,\mu}^2 \quad (36)$$

where $M = 2$ is the number of chromophores and $N = 100$ is the number of vibrational modes per chromophore (so that the overall number of nuclear DOF is $N_n = 200$). The displacements $\{D_k\}$ are assumed to be the same for each chromophore and are given by $D_k = g_k/\omega_k^2$, where $\{\omega_k\}$ and $\{g_k\}$ are obtained from the Debye spectral density

$$J(\omega) = \frac{\pi}{2}\sum_{k=1}^{N}\frac{g_k^2}{\omega_k}\delta(\omega - \omega_k) \to 2\zeta\frac{\omega\omega_c}{\omega^2 + \omega_c^2} \quad (37)$$

following the discretization approach outlined in ref 97. $\zeta = (1/2)\sum_{\mu=1}^{N}\omega_\mu^2 D_\mu^2$ and ω_c correspond to the reorganization energy and cutoff frequency, respectively.

Below, we report calculations for this model using a parameter set adopted from previous studies,[26,98] namely: $\epsilon_1 = 50$ cm^{-1}, $\epsilon_2 = -50$ cm^{-1} and $V_{12} = V_{21} = 100$ cm^{-1}, $\omega_c = 18$ cm^{-1}, and $\lambda = 50$ cm^{-1}. The initial state is assumed to be of the form of eq 12, with the temperature set to 300 K.

All three pulses are assumed to have the same polarization and shape. The envelope of the nth pulse, which is given by $\boldsymbol{E}_n(t - T_n) = \boldsymbol{\epsilon}g(t - T_n)$, is assumed to be of Gaussian form, where $g(t - T_n) = \sqrt{2\pi}\tau e^{-(t-T_n)^2/2\tau^2}$. The pulse width is set to $\tau = 40$ au $= 0.968$ fs, and the pulse carrier frequency is set to $\omega = 16\,000$ cm^{-1}. The transition dipole moments for the two sites are assumed to be *anti-parallel* with the ratio of their magnitudes given by $\mu_{01}/\mu_{02} = 5$. We also define the Rabi frequency as $\chi_0 = |\mu_{02}E_n(0)|$.

4. RESULTS AND DISCUSSION

The quantum-mechanically exact 2DES and PP spectra for the benchmark model under consideration were calculated with the HOEM method via the open-source package pyrho,[99] within the *perturbative* approach.[1] It was therefore important to establish the field parameters which correspond to the limit where third-order perturbation theory is valid. To this end, we consider the dependence of the PP and 2DES spectra at $T = 0$, as obtained via the nonperturbative approach using mLSC/$\phi^1\phi^1$, on the laser field Rabi frequency (see Figures 2 and 3). The choice of mLSC/$\phi^1\phi^1$ for this purpose is motivated by the fact that it was found to be the most accurate QC/MH method for the system under consideration (it was confirmed that similar results were obtained when using other methods). The results in Figures 2 and 3 clearly show significant deviations from the perturbative results at high values of the Rabi frequency, which are attributed to the breakdown of the weak-field approximation. However,

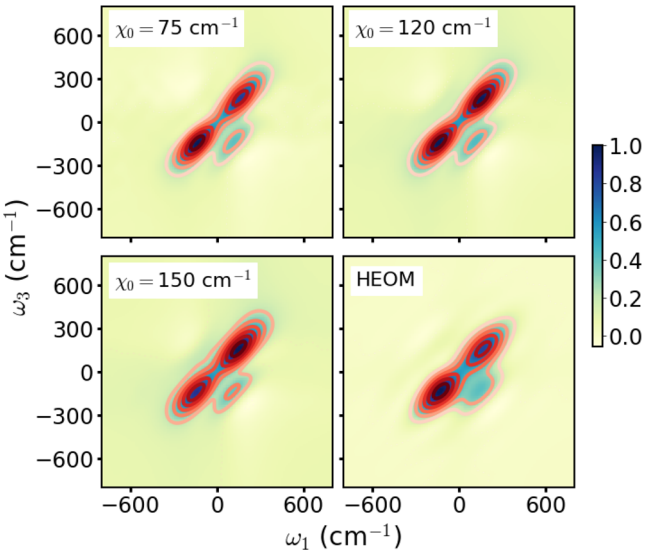

Figure 2. 2DES spectra obtained via mLSC/$\phi^1\phi^1$ at $T = 0$ fs for different values of the Rabi frequencies, $\chi_0 = |\mu_{20}g_n(0)|$. Also shown are quantum-mechanically exact results calculated via HEOM with the perturbative approach.

https://dx.doi.org/10.1021/acs.jctc.0c00843
J. Chem. Theory Comput. 2020, 16, 6491−6502

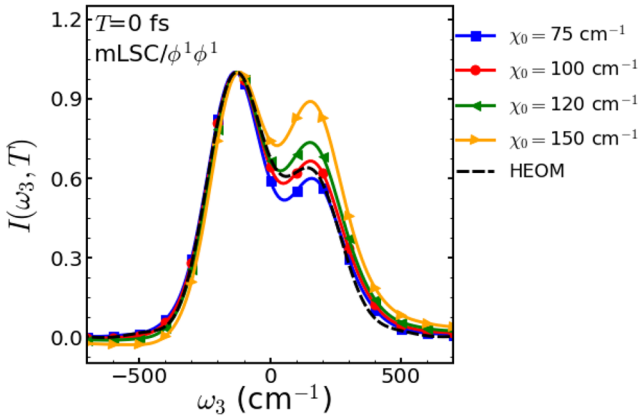

Figure 3. PP spectra obtained via mLSC/$\phi^1\phi^1$ at $T = 0$ fs for different values of the Rabi frequencies, $\chi_0 = |\mu_{20}\mathcal{E}_n(0)|$. Also shown are quantum-mechanically exact results calculated via HEOM with the perturbative approach.

those deviations are seen to diminish as the Rabi frequency is made smaller, reaching very good agreement with the perturbative results at $\chi_0 = 75$ cm^{-1}. In light of this, the Rabi frequency was set to $\chi_0 = 75$ cm^{-1} in all the calculations of 2DES and PP spectra reported below, which were done via the nonperturbative approach and based on different QC/MH methods.

2DES spectra calculated via the six different QC/MH methods under consideration in this paper are shown in Figures 4 (mLSC/$\phi^1\phi^1$, mLSC/$\phi^1\phi^2$, and mLSC/$\phi^2\phi^2$) and 5 (LCI, LCII, and MF). The corresponding PP spectra are shown in

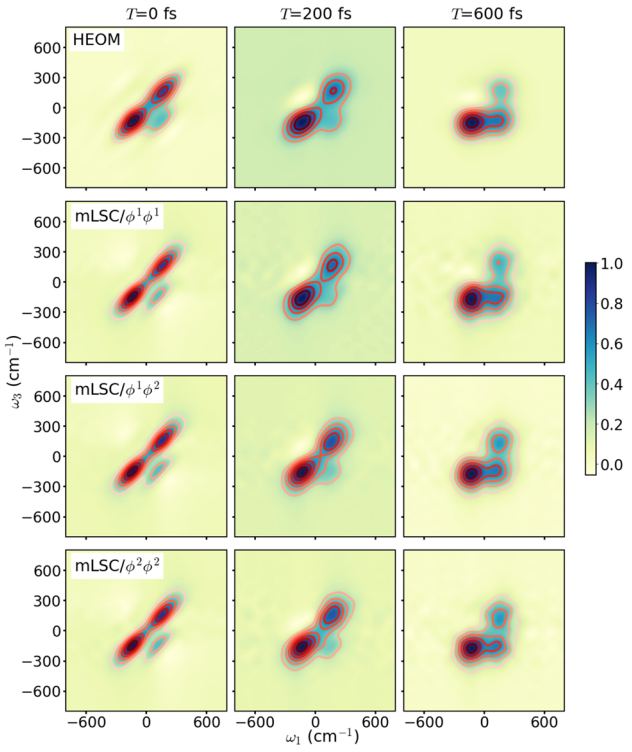

Figure 4. 2DES spectra as obtained via mLSC/$\phi^1\phi^1$, mLSC/$\phi^1\phi^2$, and mLSC/$\phi^2\phi^2$ with $\chi_0 = 75$ cm^{-1} at $T = 0$, 200, 600 fs. Also shown are quantum-mechanically exact results calculated via HEOM with the perturbative approach.

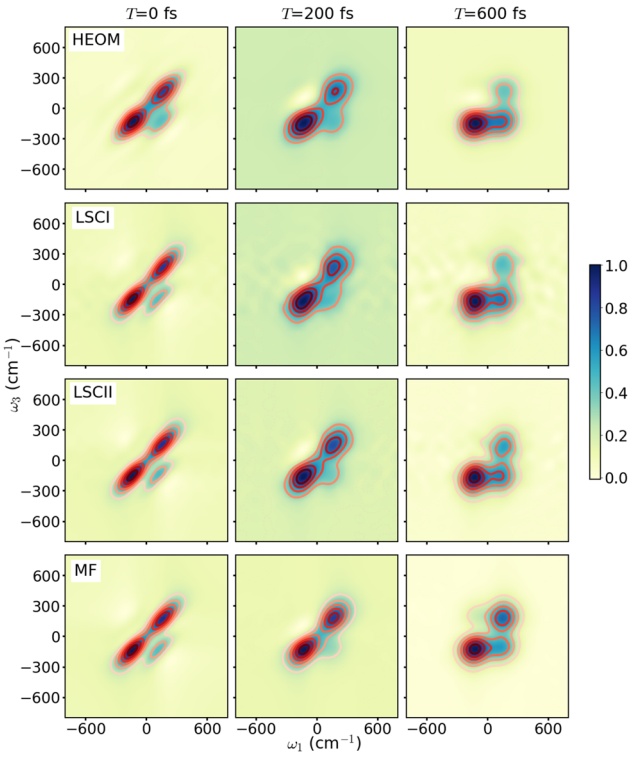

Figure 5. 2DES spectra as obtained via LCI, LCII, and MF with $\chi_0 = 75$ cm^{-1} at $T = 0$, 200, 600 fs. Also shown are quantum-mechanically exact results calculated via HEOM with the perturbative approach.

Figure 6. All spectra were calculated with $\chi_0 = 75$ cm^{-1} and are shown at three different values of the waiting time between the pump and probe pulses (PP spectra, Figure 6) or second and third pulses (2DES spectra, Figures 4-5), $T = 0$, 200, 600 fs. Also shown for comparison in those figures are the corresponding quantum-mechanically exact HEOM results. The relative growth of the low-frequency peak at the expense of the high-frequency peak in the PP spectra and the emergence of an off-diagonal peak with increasing waiting time in the 2DES spectra are indicative of energy transfer from the high-energy singly excited state to the low-energy singly excited state.

Inspection of Figures 4−6 reveals a clear hierarchy with respect to the accuracy of different QC/MH methods. The predictions of all six QC/MH methods are seen to coincide and to be in good agreement with the exact HEOM results at $T = 0$ fs. This is expected, since $T = 0$ fs corresponds to zero waiting time and is therefore minimally impacted by the approximate nuclear dynamics. However,the predictions of the different QC/MH methods are seen to deviate from one another more and more with increasing waiting time. Those deviations are clearly discernible in the PP spectra (Figure 6) but upon closer inspection can also be observed in the 2DES spectra (Figures 4 and 5). The MF method is seen to be the least accurate. The mLSC/$\phi^1\phi^1$ and LSCI methods are seen to be the most accurate and are in fact in good agreement with the exact results throughout the entire 600 fs time range considered. The LSCII, mLSC/$\phi^1\phi^2$, and mLSC/$\phi^2\phi^2$ methods are seen to outperform MF but to also be inferior in their accuracy to mLSC/$\phi^1\phi^1$ and LSCI, with significant deviations from the exact results. It is interesting to note that mLSC/$\phi^1\phi^1$ and LSCI were also recently observed to outperform other QC/MH methods in the context of electronic dynamics through conical intersections.[78]

https://dx.doi.org/10.1021/acs.jctc.0c00843
J. Chem. Theory Comput. 2020, 16, 6491−6502

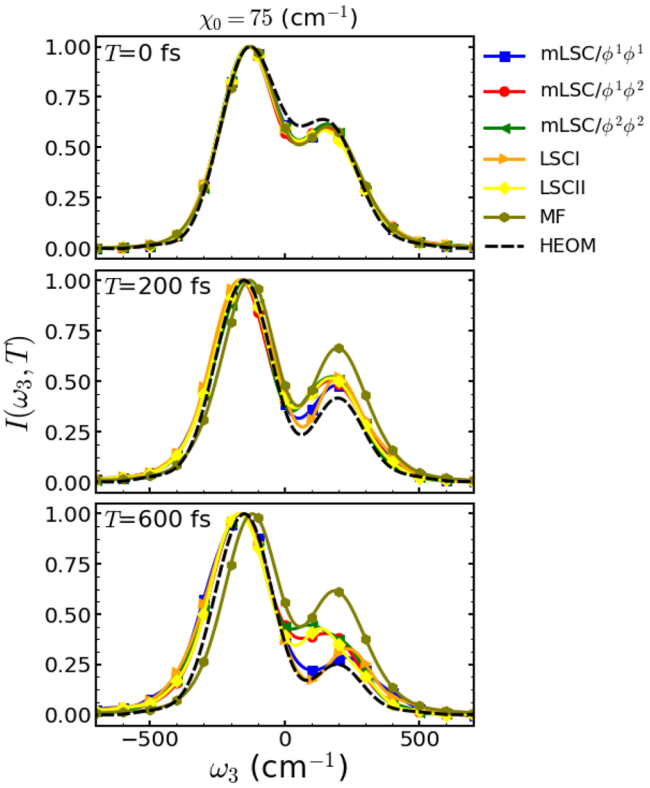

Figure 6. PP spectra obtained via mLSC/$\phi^1\phi^1$, mLSC/$\phi^1\phi^2$, mLSC/$\phi^2\phi^2$, LCI, LCII, and MF with $\chi_0 = 75$ cm^{-1} at $T = 0$, 200, 600 fs. Also shown are quantum-mechanically exact results calculated via HEOM with the perturbative approach.

In light of the superior accuracy of mLSC/$\phi^1\phi^1$ over LSCI when tested on other benchmark systems,[77] mLSC/$\phi^1\phi^1$ appears to emerge as the method of choice.

5. SUMMARY

In this paper, we presented a new methodology for simulating multidimensional electronic spectra of complex multiexcitonic molecular systems within the framework of QC/MH methods. Although the methodology was demonstrated and tested on a biexciton benchmark model where the PESs are harmonic and identical except for a shift in equilibrium geometry and energy, the methodology presented herein would be most useful for molecular systems with a large number of nuclear DOF undergoing nonequilibrium nonadiabatic dynamics on multiple coupled anharmonic electronic potential energy surfaces, for which quantum-mechanically exact methods are not feasible. The methodology is also based on a nonperturbative treatment of field−matter interaction, which is straightforward to combine with QC/MH methods and can accommodate laser fields of arbitrary shape and intensity, as dictated by experimental conditions.

The results obtained for the biexciton benchmark model are encouraging and demonstrate the ability of the new methodology to predict accurate 2DES and PP spectra. LSC-based methods are seen to be superior to MF, with the recently introduced mLSC/$\phi^1\phi^1$ implementation of the LSC approximation emerging as the most accurate and therefore the most promising for future applications.

Further benchmarking will be required for establishing the range of applicability of the new methodology. It would also be useful to apply the methodology to an all-atom anharmonic model of a system for which experimental spectra are available for comparison and interpretation. Work on such extensions is currently underway and will be reported in future publications.

AUTHOR INFORMATION

Corresponding Author

Eitan Geva − *Department of Chemistry, University of Michigan, Ann Arbor, Michigan 48109, United States;* orcid.org/0000-0002-7935-4586; Email: eitan@umich.edu

Author

Xing Gao − *Department of Chemistry, University of Michigan, Ann Arbor, Michigan 48109, United States*

Complete contact information is available at: https://pubs.acs.org/10.1021/acs.jctc.0c00843

Notes

The authors declare no competing financial interest.

ACKNOWLEDGMENTS

We thank Justin Provazza and Jonathan H. Fetherolf for helpful discussions. E.G. is grateful for support from the NSF via grants CHE-1800325 and CHE-1663636. Computational resources and services for this project were provided by Advanced Research Computing at the University of Michigan, Ann Arbor, MI.

REFERENCES

(1) Mukamel, S. *Principles of Nonlinear Optical Spectroscopy*; Oxford: New York, 1995.
(2) Jonas, D. M. Two-dimensional femtosecond spectroscopy. *Annu. Rev. Phys. Chem.* **2003**, *54*, 425−463.
(3) Cho, M. Coherent two-dimensional optical spectroscopy. *Chem. Rev.* **2008**, *108*, 1331−1418.
(4) Ogilvie, J. P.; Kubarych, K. J. Multidimensional electronic and vibrational spectroscopy: an ultrafast probe of molecular relaxation and reaction dynamics. *Adv. At., Mol., Opt. Phys.* **2009**, *57*, 249−321.
(5) Mukamel, S.; Bakker, H. J. Preface: Special Topic on Multi-dimensional Spectroscopy. *J. Chem. Phys.* **2015**, *142*, 212101−3.
(6) Ka, B. J.; Geva, E. A nonperturbative calculation of nonlinear spectroscopic signals in liquid solution. *J. Chem. Phys.* **2006**, *125*, 214501−14.
(7) McRobbie, P. L.; Geva, E. A benchmark study of different methods for calculating one- and two-dimensional optical spectra. *J. Phys. Chem. A* **2009**, *113*, 10425−10434.
(8) McRobbie, P. L.; Hanna, G.; Shi, Q.; Geva, E. Signatures of nonequilibrium solvation dynamics on multi-dimensional spectra. *Acc. Chem. Res.* **2009**, *42*, 1299−1309.
(9) Hanna, G.; Geva, E. Computational study of the one and two dimensional infrared spectra of a vibrational mode strongly coupled to its environment: Beyond the cumulant and Condon approximations. *J. Phys. Chem. B* **2008**, *112*, 12991−13004.
(10) Hanna, G.; Geva, E. Isotope Effects on the Vibrational Relaxation and Multidimensional Infrared Spectra of the Hydrogen Stretch in a Hydrogen-Bonded Complex Dissolved in a Polar Liquid. *J. Phys. Chem. B* **2008**, *112*, 15793−15800.
(11) Hanna, G.; Geva, E. Multi-dimensional spectra via the mixed quantum-classical Liouville method: Signatures of nonequilibrium dynamics. *J. Phys. Chem. B* **2009**, *113*, 9278−9288.
(12) Hanna, G.; Geva, E. Computational study of the signature of hydrogen-bond strength on the infrared spectra of a hydrogen-bonded complex dissolved in a polar liquid. *Chem. Phys.* **2010**, *370*, 201.
(13) Hanna, G.; Geva, E. Signature of Nonadiabatic Transitions on the Pump-Probe Infrared Spectra of a Hydrogen-Bonded Complex Dissolved in a Polar Solvent: A Computational Study. *J. Phys. Chem. B* **2011**, *115*, 5191−5200.

(14) Baiz, C. R.; Kubarych, K. J.; Geva, E.; McRobbie, P. L.; Preketes, N. K. Two-dimensional infrared spectroscopy of dimanganese decacarbonyl and its photoproducts: An ab-initio study. *J. Phys. Chem. A* **2009**, *113*, 9617.
(15) Baiz, C. R.; Kubarych, K. J.; Geva, E. Molecular theory and simulation of coherence transfer in metal carbonyls and its signature on multidimensional infrared spectra. *J. Phys. Chem. B* **2011**, *115*, 5322−5339.
(16) Kwac, K.; Geva, E. Mixed Quantum-Classical Molecular Dynamics Study of the Hydroxyl Stretch in Methanol/Carbon-Tetrachloride Mixtures II: Excited State Hydrogen Bonding Structure and Dynamics, Infrared Emission Spectrum and Excited State Life-Time. *J. Phys. Chem. B* **2012**, *116*, 2856−2866.
(17) Kwac, K.; Geva, E. A Mixed Quantum-Classical Molecular Dynamics Study of the Hydroxyl Stretch in Methanol/Carbon Tetrachloride Mixtures III: Nonequilibrium Hydrogen-Bond Dynamics and Infrared Pump-Probe Spectra. *J. Phys. Chem. B* **2013**, *117*, 7737−7749.
(18) Kwac, K.; Geva, E. A Mixed Quantum-Classical Molecular Dynamics Study of anti-Tetrol and syn-Tetrol Dissolved in Liquid Chloroform: Hydrogen-Bond Structure and Its Signature on the Infrared Absorption Spectrum. *J. Phys. Chem. B* **2013**, *117*, 9996−10006.
(19) Kwac, K.; Geva, E. A Mixed Quantum-Classical Molecular Dynamics Study of anti-Tetrol and syn-Tetrol Dissolved in Liquid Chloroform II: Infrared Emission Spectra, Vibrational Excited-State Life-Times and Nonequilibrium Hydrogen-Bond Dynamics. *J. Phys. Chem. B* **2013**, *117*, 14457−14467.
(20) Bai, S.; Xie, W.; Zhu, L.; Shi, Q. Calculation of absorption spectra involving multiple excited states: Approximate methods based on the mixed quantum classical Liouville equation. *J. Chem. Phys.* **2014**, *140*, 084105.
(21) Gruenbaum, S. M.; Loring, R. F. Semiclassical mean-trajectory approximation for nonlinear spectroscopic response functions. *J. Chem. Phys.* **2008**, *129*, 124510.
(22) Petit, A. S.; Subotnik, J. E. Appraisal of surface hopping as a tool for modeling condensed phase linear absorption spectra. *J. Chem. Theory Comput.* **2015**, *11*, 4328−4341.
(23) Jain, A.; Petit, A. S.; Anna, J. M.; Subotnik, J. E. Simple and Efficient Theoretical Approach To Compute 2D Optical Spectra. *J. Phys. Chem. B* **2019**, *123*, 1602−1617.
(24) Van Der Vegte, C.; Dijkstra, A.; Knoester, J.; Jansen, T. Calculating two-dimensional spectra with the mixed quantum-classical ehrenfest method. *J. Phys. Chem. A* **2013**, *117*, 5970−5980.
(25) Tempelaar, R.; van der Vegte, C. P.; Knoester, J.; Jansen, T. L. Surface hopping modeling of two-dimensional spectra. *J. Chem. Phys.* **2013**, *138*, 164106.
(26) Provazza, J.; Segatta, F.; Garavelli, M.; Coker, D. F. Semiclassical path integral calculation of nonlinear optical spectroscopy. *J. Chem. Theory Comput.* **2018**, *14*, 856−866.
(27) Richter, M.; Fingerhut, B. P. Simulation of multi-dimensional signals in the optical domain: Quantum-classical feedback in nonlinear exciton propagation. *J. Chem. Theory Comput.* **2016**, *12*, 3284−3294.
(28) Seidner, L.; Stock, G.; Domcke, W. Nonperturbative approach to femtosecond spectroscopy: General theory and application to multi-dimensional nonadiabatic photoisomerization processes. *J. Chem. Phys.* **1995**, *103*, 3998−4011.
(29) Tian, P.; Keusters, D.; Suzaki, Y.; Warren, W. S. Femtosecond phase-coherent two-dimensional spectroscopy. *Science* **2003**, *300*, 1553−1555.
(30) Tan, H. S. Theory and phase-cycling scheme selection principles of collinear phase coherent multi-dimensional optical spectroscopy. *J. Chem. Phys.* **2008**, *129*, 124501−14.
(31) Yan, S.; Tan, H. S. Phase cycling schemes for two-dimensional optical spectroscopy with a pump−probe beam geometry. *Chem. Phys.* **2009**, *360*, 110−115.
(32) Bloem, R.; Garrett-Roe, S.; Strzalka, H.; Hamm, P.; Donaldson, P. Enhancing signal detection and completely eliminating scattering using quasi-phase-cycling in 2D IR experiments. *Opt. Express* **2010**, *18*, 27067−27078.
(33) Zhang, Z.; Wells, K. L.; Hyland, E. W. J.; Tan, H. S. Phase-cycling schemes for pump−probe beam geometry two-dimensional electronic spectroscopy. *Chem. Phys. Lett.* **2012**, *550*, 156−161.
(34) Mančal, T.; Pisliakov, A. V.; Fleming, G. R. Three-dimensional optical three-pulse photon echo spectroscopy. I. Nonperturbative approach to the calculation of spectra. *J. Chem. Phys.* **2006**, *124*, 234504.
(35) Wang, H.; Thoss, M. Nonperturbative quantum simulation of time-resolved nonlinear spectra: Methodology and application to electron transfer reactions in the condensed phase. *Chem. Phys.* **2008**, *347*, 139−151.
(36) Meyer, S.; Engel, V. Non-perturbative wave-packet calculations of time-resolved four-wave-mixing signals. *Appl. Phys. B: Lasers Opt.* **2000**, *71*, 293−297.
(37) Keß, M.; Worth, G.; Engel, V. Two-dimensional vibronic spectroscopy of molecular aggregates: Trimers, dimers, and monomers. *J. Chem. Phys.* **2016**, *145*, 084305.
(38) Tamura, H.; Burghardt, I.; Tsukada, M. Exciton Dissociation at Thiophene/Fullerene Interfaces: The Electronic Structures and Quantum Dynamics. *J. Phys. Chem. C* **2011**, *115*, 10205−10210.
(39) Lee, M. H.; Dunietz, B. D.; Geva, E. Calculation From First Principles of Intramolecular Golden-Rule Rate Constants for Photo-Induced Electron Transfer in Molecular Donor-Acceptor Systems. *J. Phys. Chem. C* **2013**, *117*, 23391−23401.
(40) Lee, M. H.; Dunietz, B. D.; Geva, E. Calculation from First Principles of Golden-Rule Rate Constants for Photo-Induced Subphthalocyanine/Fullerene Interfacial Charge Transfer and Recombination in Organic Photovoltaic Cells. *J. Phys. Chem. C* **2014**, *118*, 9780−9789.
(41) Lee, M. H.; Dunietz, B. D.; Geva, E. Donor-to-Donor vs. Donor-to-Acceptor Interfacial Charge Transfer States in the Phthalocyanine-Fullerene Organic Photovoltaic System. *J. Phys. Chem. Lett.* **2014**, *5*, 3810−3816.
(42) Lee, M. K.; Coker, D. F. Modeling Electronic-Nuclear Interactions for Excitation Energy Transfer Processes in Light-Harvesting Complexes. *J. Phys. Chem. Lett.* **2016**, *7*, 3171−3178.
(43) Novoderezhkin, V. I.; Romero, E.; Dekker, J. P.; van Grondelle, R. Multiple Charge-Separation Pathways in Photosystem II: Modeling of Transient Absorption Kinetics. *ChemPhysChem* **2011**, *12*, 681−688.
(44) Chandrasekaran, S.; Aghtar, M.; Valleau, S.; Aspuru-Guzik, A.; Kleinekathöfer, U. Influence of Force Fields and Quantum Chemistry Approach on Spectral Densities of BChl a in Solution and in FMO Proteins. *J. Phys. Chem. B* **2015**, *119*, 9995−10004.
(45) Gottwald, F.; Ivanov, S. D.; Kühn, O. Applicability of the Caldeira-Leggett Model to Vibrational Spectroscopy in Solution. *J. Phys. Chem. Lett.* **2015**, *6*, 2722−2727.
(46) Nitzan, A. *Chemical Dynamics in Condensed Phases*; Oxford University Press: New York, 2006.
(47) Wang, H.; Thoss, M. Quantum Dynamical Simulation of Electron-Transfer Reactions in an Anharmonic Environment. *J. Phys. Chem. A* **2007**, *111*, 10369−10375.
(48) López-López, S.; Martinazzo, R.; Nest, M. Benchmark calculations for dissipative dynamics of a system coupled to an anharmonic bath with the multiconfiguration time-dependent Hartree method. *J. Chem. Phys.* **2011**, *134*, 094102−8.
(49) Hsieh, C.-Y.; Kapral, R. Correlation Functions in Open Quantum-Classical Systems. *Entropy* **2014**, *16*, 200−220.
(50) Kwac, K.; Geva, E. A Mixed Quantum-Classical Molecular Dynamics Study of the Hydroxyl Stretch in Methanol/Carbon Tetrachloride Mixtures: Equilibrium Hydrogen-Bond Structure and Dynamics at the Ground State and the Infrared Absorption Spectrum. *J. Phys. Chem. B* **2011**, *115*, 9184−9194.
(51) van der Vegte, C. P.; Dijkstra, A. G.; Knoester, J.; Jansen, T. L. C. Calculating Two-Dimensional Spectra with the Mixed Quantum-Classical Ehrenfest Method. *J. Phys. Chem. A* **2013**, *117*, 5970−5980.
(52) Loring, R. F. Mean-trajectory approximation for electronic and vibrational-electronic nonlinear spectroscopy. *J. Chem. Phys.* **2017**, *146*, 144106.

https://dx.doi.org/10.1021/acs.jctc.0c00843
J. Chem. Theory Comput. 2020, 16, 6491−6502

(53) Polley, K.; Loring, R. F. Two-dimensional vibronic spectra from classical trajectories. *J. Chem. Phys.* **2019**, *150*, 164114.
(54) Provazza, J.; Coker, D. F. Communication: Symmetrical quasi-classical analysis of linear optical spectroscopy. *J. Chem. Phys.* **2018**, *148*, 181102−4.
(55) Meyer, H. D.; Miller, W. H. A classical analog for electronic degrees of freedom in nonadiabatic collision processes. *J. Chem. Phys.* **1979**, *70*, 3214−3223.
(56) Stock, G.; Thoss, M. Semiclassical Description of Nonadiabatic Quantum Dynamics. *Phys. Rev. Lett.* **1997**, *78*, 578−581.
(57) Sun, X.; Wang, H.; Miller, W. H. Semiclassical theory of electronically nonadiabatic dynamics: Results of a linearized approximation to the initial value representation. *J. Chem. Phys.* **1998**, *109*, 7064.
(58) Wang, H.; Song, X.; Chandler, D.; Miller, W. H. Semiclassical study of electronically nonadiabatic dynamics in the condensed-phase: Spin-boson problem with Debye spectral density. *J. Chem. Phys.* **1999**, *110*, 4828−4840.
(59) Nassimi, A.; Bonella, S.; Kapral, R. Analysis of the quantum-classical Liouville equation in the mapping basis. *J. Chem. Phys.* **2010**, *133*, 134115−11.
(60) Swenson, D. W. H.; Levy, T.; Cohen, G.; Rabani, E.; Miller, W. H. Application of a semiclassical model for the second-quantized many-electron Hamiltonian to nonequilibrium quantum transport: The resonant level model. *J. Chem. Phys.* **2011**, *134*, 164103−9.
(61) Kelly, A.; van Zon, R.; Schofield, J.; Kapral, R. Mapping quantum-classical Liouville equation: Projectors and trajectories. *J. Chem. Phys.* **2012**, *136*, 084101−13.
(62) Cotton, S. J.; Miller, W. H. Symmetrical windowing for quantum states in quasi-classical trajectory simulations: Application to electronically non-adiabatic processes. *J. Chem. Phys.* **2013**, *139*, 234112−10.
(63) Cotton, S. J.; Miller, W. H. Symmetrical Windowing for Quantum States in Quasi-Classical Trajectory Simulations. *J. Phys. Chem. A* **2013**, *117*, 7190−7194.
(64) Cotton, S. J.; Igumenshchev, K.; Miller, W. H. Symmetrical windowing for quantum states in quasi-classical trajectory simulations: Application to electron transfer. *J. Chem. Phys.* **2014**, *141*, 084104−11.
(65) Cotton, S. J.; Miller, W. H. A Symmetrical Quasi-Classical Spin-Mapping Model for the Electronic Degrees of Freedom in Non-Adiabatic Processes. *J. Phys. Chem. A* **2015**, *119*, 12138−12145.
(66) Cotton, S. J.; Miller, W. H. The Symmetrical Quasi-Classical Model for Electronically Non-Adiabatic Processes Applied to Energy Transfer Dynamics in Site-Exciton Models of Light-Harvesting Complexes. *J. Chem. Theory Comput.* **2016**, *12*, 983−991.
(67) Cotton, S. J.; Miller, W. H. A new symmetrical quasi-classical model for electronically non-adiabatic processes: Application to the case of weak non-adiabatic coupling. *J. Chem. Phys.* **2016**, *145*, 144108−17.
(68) Saller, M. A. C.; Kelly, A.; Richardson, J. O. On the identity of the identity operator in nonadiabatic linearized semiclassical dynamics. *J. Chem. Phys.* **2019**, *150*, 071101−8.
(69) Saller, M. A. C.; Kelly, A.; Richardson, J. O. Improved population operators for multi-state nonadiabatic dynamics with the mixed quantum-classical mapping approach. *Faraday Discuss.* **2020**, *221*, 150−167.
(70) Tao, G. Electronically Nonadiabatic Dynamics in Singlet Fission: A Quasi-Classical Trajectory Simulation. *J. Phys. Chem. C* **2014**, *118*, 17299−17305.
(71) Tao, G. A multi-state trajectory method for non-adiabatic dynamics simulations. *J. Chem. Phys.* **2016**, *144*, 094108−9.
(72) Tao, G.; Shen, N. Mapping State Space to Quasiclassical Trajectory Dynamics in Coherence-Controlled Nonadiabatic Simulations for Condensed Phase Problems. *J. Phys. Chem. A* **2017**, *121*, 1734−1747.
(73) Tao, G. Nonadiabatic Dynamics of Hydrogen Diffusion on Cu(001): Classical Mapping Model with Multistate Projection Window in Real Space. *ChemPhysChem* **2019**, *62*, 39−9.
(74) Liu, J. A unified theoretical framework for mapping models for the multi-state Hamiltonian. *J. Chem. Phys.* **2016**, *145*, 204105−15.
(75) Kananenka, A. A.; Hsieh, C.-Y.; Cao, J.; Geva, E. Nonadiabatic Dynamics via the Symmetrical Quasi-Classical Method in the Presence of Anharmonicity. *J. Phys. Chem. Lett.* **2018**, *9*, 319−326.
(76) He, X.; Liu, J. A new perspective for nonadiabatic dynamics with phase space mapping models. *J. Chem. Phys.* **2019**, *151*, 024105−22.
(77) Gao, X.; Saller, M. A. C.; Liu, Y.; Kelly, A.; Richardson, J. O.; Geva, E. Benchmarking Quasiclassical Mapping Hamiltonian Methods for Simulating Electronically Nonadiabatic Molecular Dynamics. *J. Chem. Theory Comput.* **2020**, *16*, 2883−2895.
(78) Liu, Y.; Gao, X.; Lai, Y.; Mulvihill, E.; Geva, E. Electronic Dynamics through Conical Intersections via Quasiclassical Mapping Hamiltonian Methods. *J. Chem. Theory Comput.* **2020**, *16*, 4479−4488.
(79) Meyer, H.-D.; Gatti, F.; Worth, G. A. *Multidimensional Quantum Dynamics; MCTDH Theory and Applications*; John Wiley & Sons: New York, 2009.
(80) Miller, W. H.; Cotton, S. J. Classical molecular dynamics simulation of electronically non-adiabatic processes. *Faraday Discuss.* **2016**, *195*, 9−30.
(81) Gao, X.; Lai, Y.; Geva, E. Simulating Absorption Spectra of Multi-Excitonic Systems via Quasiclassical Mapping Hamiltonian Methods. *J. Chem. Theory Comput.* **2020**, DOI: 10.1021/acs.jctc.0c00709.
(82) Ishizaki, A.; Fleming, G. R. On the adequacy of the Redfield equation and related approaches to the study of quantum dynamics in electronic energy transfer. *J. Chem. Phys.* **2009**, *130*, 234110−9.
(83) Kananenka, A. A.; Sun, X.; Schubert, A.; Dunietz, B. D.; Geva, E. A comparative study of different methods for calculating electronic transition rates. *J. Chem. Phys.* **2018**, *148*, 102304−13.
(84) Thoss, M.; Stock, G. Mapping approach to the semiclassical description of nonadiabatic quantum dynamics. *Phys. Rev. A: At., Mol., Opt. Phys.* **1999**, *59*, 64−79.
(85) Stock, G.; Müller, U. Flow of zero-point energy and exploration of phase space in classical simulations of quantum relaxation dynamics. *J. Chem. Phys.* **1999**, *111*, 65−76.
(86) Miller, W. H. The semiclassical initial value representation: A potentially practical way for adding quantum effects to classical molecular dynamics simulations. *J. Phys. Chem. A* **2001**, *105*, 2942−2955.
(87) Ananth, N.; Venkataraman, C.; Miller, W. H. Semiclassical description of electronically nonadiabatic dynamics via the initial value representation. *J. Chem. Phys.* **2007**, *127*, 084114−10.
(88) Kim, H.; Nassimi, A.; Kapral, R. Quantum-classical Liouville dynamics in the mapping basis. *J. Chem. Phys.* **2008**, *129*, 084102.
(89) Miller, W. H.; Cotton, S. J. Communication: Wigner functions in action-angle variables, Bohr-Sommerfeld quantization, the Heisenberg correspondence principle, and a symmetrical quasi-classical approach to the full electronic density matrix. *J. Chem. Phys.* **2016**, *145*, 081102−5.
(90) Cotton, S. J.; Liang, R.; Miller, W. H. On the adiabatic representation of Meyer-Miller electronic-nuclear dynamics. *J. Chem. Phys.* **2017**, *147*, 064112−11.
(91) Wang, H.; Thoss, M.; Miller, W. H. Forward-backward initial value representation for the calculation of thermal rate constants for reactions in complex molecular systems. *J. Chem. Phys.* **2000**, *112*, 47.
(92) Shi, Q.; Geva, E. A relationship between semiclassical and centroid correlation functions. *J. Chem. Phys.* **2003**, *118*, 8173−8184.
(93) Shi, Q.; Geva, E. Nonradiative electronic relaxation rate constants from approximations based on linearizing the path-integral forward-backward action. *J. Phys. Chem. A* **2004**, *108*, 6109−6116.
(94) Runeson, J. E.; Richardson, J. O. Spin-mapping approach for nonadiabatic molecular dynamics. *J. Chem. Phys.* **2019**, *151*, 044119.
(95) Mulvihill, E.; Gao, X.; Liu, Y.; Schubert, A.; Dunietz, B. D.; Geva, E. Combining the mapping Hamiltonian linearized semiclassical approach with the generalized quantum master equation to simulate electronically nonadiabatic molecular dynamics. *J. Chem. Phys.* **2019**, *151*, 074103.
(96) Zhang, P.-P.; Eisfeld, A. Non-Perturbative Calculation of Two-Dimensional Spectra Using the Stochastic Hierarchy of Pure States. *J. Phys. Chem. Lett.* **2016**, *7*, 4488−4494.

(97) Wang, Z.; Pakoulev, A.; Pang, Y.; Dlott, D. D. Vibrational substructure in the OH stretching bend in water. *Chem. Phys. Lett.* **2003**, *378*, 281.
(98) Fetherolf, J. H.; Berkelbach, T. C. Linear and nonlinear spectroscopy from quantum master equations. *J. Chem. Phys.* **2017**, *147*, 244109.
(99) Berkelbach, T. *Pyrho: A python package for reduced density matrix techniques*; https://github.com/berkelbach-group/pyrho.

https://dx.doi.org/10.1021/acs.jctc.0c00843
J. Chem. Theory Comput. 2020, 16, 6491−6502